FIREBALL ENTRAINMENT STUDY

Wayne W. Haigh, et al

TRW Systems Group

Prepared for:

Defense Nuclear Agency

November 1973

Unclassified

SECURITY CLASSIFICATION OF THIS PAGE (When Data Entered)

AD-771276

REPORT DOCUMENTATION PAGE

READ INSTRUCTIONS BEFORE COMPLETING FORM

1 REPORT NUMBER: DNA 3139Z	2 GOVT ACCESSION NO.
3 RECIPIENT'S CATALOG NUMBER	
4 TITLE (and Subtitle): Fireball Entrainment Study	5 TYPE OF REPORT & PERIOD COVERED: Semi-Annual Report 1 August 1973 - 30 April 1973
6 PERFORMING ORG. REPORT NUMBER: 18895-6003-RU-00	
7 AUTHOR(s): Wayne W. Haigh and David D. Mantrom	8 CONTRACT OR GRANT NUMBER(s): DNA001-72-C-0019
9 PERFORMING ORGANIZATION NAME AND ADDRESS: TRW Systems Group, One Space Park, Redondo Beach, California 90278	10 PROGRAM ELEMENT, PROJECT, TASK AREA & WORK UNIT NUMBERS: ARPA Order No. 1433, Subtask No. ZL433, Work Unit No. 08
11 CONTROLLING OFFICE NAME AND ADDRESS: Director, Defense Advanced Research Projects Agency, Washington, D. C. 20301	12 REPORT DATE: November 1973 13 NUMBER OF PAGES: 45
14 MONITORING AGENCY NAME & ADDRESS (if different from Controlling Office): Director, Defense Nuclear Agency, Washington, D. C. 20305	15 SECURITY CLASS (of this report): Unclassified 15a DECLASSIFICATION DOWNGRADING SCHEDULE

16 DISTRIBUTION STATEMENT (of this Report)

Approved for public release; distribution unlimited.

17 DISTRIBUTION STATEMENT (of the abstract entered in Block 20, if different from Report)

18 SUPPLEMENTARY NOTES

19 KEY WORDS (Continue on reverse side if necessary and identify by block number)

Entrainment
Fireballs
Turbulent Mixing
Holographic Interferometry
Fireball Experiments

20 ABSTRACT (Continue on reverse side if necessary and identify by block number)

A continuation of an experimental program to study the process of entrainment and turbulent mixing in fireballs is described. Recent modifications and additions to the experimental facility are discussed. Both laminar and turbulent helium concentration data are presented, reduced by an ensemble averaging technique based on physical features of the flow field. Laboratory turbulent size/rise data are presented and are shown to be in excellent agreement with data from a low altitude, low yield nuclear test. Photographs of particulate seeded vortices show a distinct "jelly-roll" structure at a

DD FORM 1 JAN 73 1473 EDITION OF 1 NOV 65 IS OBSOLETE

Unclassified

SECURITY CLASSIFICATION OF THIS PAGE (When Data Entered)

Abstract (Continued)

laminar condition whereas turbulent mixing in higher Reynolds number events is shown to overwhelm that structure.

DNA 3139Z

FIREBALL ENTRAINMENT STUDY

Wayne W. Haigh
and
David D. Mantrom

November 1973

Semi-Annual Report for Period 1 August 1972 - 30 April 1973

Contract No. DNA001-72-C-0019

Sponsored by

Defense Advanced Research Projects Agency
ARPA Order No. 1433
Work Unit 08

This work was supported by the
Defense Nuclear Agency under
Subtask HC061-08

Prepared for
Director, Defense Nuclear Agency
Washington, D. C. 20305

TRW
SYSTEMS GROUP
ONE SPACE PARK, REDONDO BEACH, CALIFORNIA 90278

FOREWORD

This research was supported by the Advanced Research Projects Agency and was monitored by the Defense Nuclear Agency, under ARPA Order No. 1433 and Contract DNA 001-72-C-0019.

The views and conclusions contained in this document are those of the authors and should not be interpreted as necessarily representing the official policies, either expressed or implied, of the Advanced Research Projects Agency or the U. S. Government.

TABLE OF CONTENTS

		Page
1.	INTRODUCTION	1
2.	EXPERIMENTAL FACILITY	2
	2.1 Helium Release System	2
	2.2 Particle Tracking System	2
	2.2.1 Particulate-Seeded Bubbles	2
	2.2.2 Camera/Flash System	4
3.	DATA ACQUISITION AND INTERPRETATION	9
	3.1 Acquisition and Interpretation of Finite Fringe Interferograms	9
	3.2 Acquisition and Interpretation of Particle Tracking Data	10
4.	DATA REDUCTION	12
	4.1 Holographic Infinite Fringe Interferometry Data	12
	4.1.1 Establishment of Coordinates on Individual Interferograms	13
	4.1.2 Obtaining Fringe Profiles from Individual Interferograms	14
	4.1.3 Data Averaging	14
	4.1.4 Fireball Wake Interferometry Data Reduction	17
	4.2 Holographic Finite Fringe Interferometry Data	18
	4.3 Shadowgraph Data	18
5.	EXPERIMENTAL RESULTS	24
	5.1 Holographic Interferometry Data	24
	5.1.1 Laminar Results	24
	5.1.2 Turbulent Results	25
	5.2 Shadowgraph Size/Rise Statistics	26
	5.3 Particle Tracking Results	26
6.	CURRENT STATUS AND FUTURE PLANS	37
7.	REFERENCES	38

LIST OF ILLUSTRATIONS

		Page
1.	High Pressure Test Facility, Holocamera, and Support Equipment.	6
2.	Schematic Diagram of Bubble Forming and Bursting System. .	7
3.	Dependence of Particulate Path on Parameter λ_o (Reference 2).	8
4.	Typical Eight Atmosphere Finite Fringe Interferogram . . .	11
5.	Finite Fringe Interferogram of Unbroken Bubble	11
6.	Nomenclature and Axes for Infinite Fringe Interferometry Data Reduction	21
7.	Nomenclature and Axes for Wake Data Reduction.	22
8.	Nomenclature and Axes for Shadowgraph Data Reduction . . .	23
9.	Typical Laminar Infinite Fringe Interferogram.	27
10.	Typical Laminar Infinite Fringe Interferogram.	27
11.	Averaged Radial Fringe Distributions - Laminar Data. . . .	28
12.	Averaged Radial Helium Concentrations - Laminar Data . . .	29
13.	Averaged Laminar Fireball Wake Helium Concentration Profiles	30
14.	Typical Turbulent Infinite Fringe Interferogram.	31
15.	Typical Turbulent Infinite Fringe Interferogram.	31
16.	Averaged Radial Fringe Distributions - Turbulent Data. . .	32
17.	Averaged Radial Helium Concentrations - Turbulent Data . .	33
18.	Fireball Size/Rise Characteristics	34
19.	Multiple Exposure Photograph of Particulate Seeded Laminar Fireball	35
20.	Multiple Exposure Photograph of Particulate Seeded Turbulent Fireball	36

1. INTRODUCTION

The prediction of radar and optical signatures resulting from atmospheric nuclear detonations requires reliable fireball entrainment and mixing models. Essential to these predictions is a sound knowledge of the temperature, chemical species, and velocity fields which are not provided by available data from nuclear tests. The objective of this program is to investigate turbulent mixing and entrainment of air in fireballs by means of a subscale laboratory simulation which will provide a data base to support the development and evaluation of theoretical fireball models and codes.

The development of fireballs from low yield (<100 kt) bursts at low altitudes (<30 km) will be dominated by buoyancy forces. The initial stage of these fireballs resulting from large energy release within the atmosphere is characterized by spherical symmetry, the domination of radiative energy transport, and the propagation of a strong spherical shock wave. On the order of a second after detonation, the fireball comes to pressure equilibrium with the ambient air and because of its low density, begins to rise. As the fireball rises, circulation is generated and a toroid is formed. The series of laboratory experiments currently being performed are designed to simulate these "buoyant rise" fireballs after pressure equilibration.

This report includes descriptions of the hardware and instrumentation added to the test facility during the last eight months. In addition, a new ensemble averaging data reduction technique is described in detail and reduced interferometry, shadowgraph, and particle tracking data are presented. Many aspects of the current investigation were discussed in detail in Reference 1 and are not repeated in this report. These topics include a support analysis and a full description of the high pressure test facility and holographic interferometer. In addition, techniques for both interferometry data acquisition and Abel inversion data reduction were described.

2. EXPERIMENTAL FACILITY

Several modifications have been made to the experimental facility since it was described in the previous Semi-Annual Report (Reference 1). The more notable among these involve the remote controlled bursting of the helium-filled soap bubbles and the addition of a particle seeding and tracking system. A photograph of the present overall experimental facility including the high pressure test tank, holocamera, and other support equipment and diagnostic instruments appears in Figure 1.

2.1 HELIUM RELEASE SYSTEM

As a result of large initial asymmetries present in vortices generated by electrical discharge bubble breaking, a mechanical breaking technique was developed which repeatedly produces a symmetric helium release. This technique consists of remotely dropping a 125 mil stainless steel sphere from an electromagnet mounted inside the tank through the top center of the bubble. Tests with no bubble have shown that no more than 1/16" dispersion from the target ever exists and interferograms taken just milliseconds after arrival of the sphere at all test pressures indicate that the helium release is indeed symmetric. A schematic of the new bubble bursting arrangement is displayed in Figure 2.

2.2 PARTICLE TRACKING SYSTEM

Equipment providing the capability of obtaining multiple exposure photographs of a rising vortex with its initial bubble seeded with a particulate tracer has recently been developed and incorporated in the test facility. It consists basically of two parts: an additional bubble formation system, and a camera/flash system.

2.2.1 Particulate-Seeded Bubbles

Several different types of flow tracers were tested, such as talcum powder, fine aluminum flakes, smoke, and hollow epoxy microspheres. Smoke was discarded since it could not be generated at the high operating

pressures, talcum powder could not be photographed, and aluminum flakes prohibited repeatable bubble formation. Consequently, epoxy microspheres from 10 to 250 microns in diameter were incorporated as the tracing particulate.

To be an effective fluid tracer, the particles used must possess relatively low inertias and high drags to follow the streamlines accurately. At the same time, they must be sufficiently large to become visible under intense illumination. Particle tracking is particularly valuable to describe flow patterns not easily accessible to other, more standard methods of measurement. The utility of this method depends on the accuracy of streamline tracing desired.

Assuming negligible radial velocities and net external forces, and using Oseen's approximation for $C_D(Re)$, results from an analysis by Wright (Reference 2) show that the path dependence of a particle in a vortex may be characterized by a single parameter,

$$\lambda_o = \frac{R_o}{V_o}\left(\frac{6\pi a \mu D_o}{M'}\right)$$

where R_o = initial position of particle from center of core of vortex

V_o = initial fluid speed

a = radius of particle

μ = fluid viscosity

D_o = drag parameter = $\frac{C_D Re}{24} = 1 + 0.1875(Re) - 0.0148(Re)^2 + \ldots$ (Reference 3)

M' = apparent mass of particle = $\frac{4}{3}\pi a^3(\rho_p + \frac{1}{2}\rho)$

ρ_p = density of particle

ρ = fluid density

A plot of this particle path dependence on parameter λ_o from Reference 2 is presented in Figure 3. It is evident that large λ_o is desirable.

For the particles used in this study, a value of λ_o may easily be computed. An example is presented to illustrate what happens to a 100μ diameter particle within a vortex having a core radius of one inch, a circumferential velocity of one ft/sec, and the fluid predominantly air at one atmosphere. The particle Reynolds number for this case is calculated to be 2, thus the drag parameter D_o using Oseen's approximation is 1.33. For this particular case, $\lambda_o \approx 14$ which is indicative of a very good tracer. Since D_o increases strongly with Re whereas M' is very weakly dependent on Re, the particulate becomes a better tracer in the higher pressure regimes.

Two features of the bubble blowing arrangement described in Reference 1 prevented its use in forming bubbles seeded with particulate. First, the helium-particulate orifice in the bubble tube head was too small and repeatedly clogged with soap and particulate. Secondly, with a larger orifice, one could not obtain a soap film over the top of the head to enable a bubble to be initiated. For these reasons, a new bubble tube head and mechanical soap applier were developed and incorporated. A schematic of the bubble blowing arrangement with the particulate mixer appearing in dashed lines is also presented as part of Figure 2.

2.2.2 Camera/Flash System

A 35mm Nikon F with motor drive having an f5.6 macro lens was selected as the optimum available camera to acquire the particle tracking photographs. Kodak Tri-X Pan (ASA 400) was chosen for film, and a special processing technique using Acufine developer was incorporated which effectively increased the speed of the film to ASA 1250, noticeably enhancing the resolution above that obtainable using standard developers.

A 7.5kV power supply operating at an energy level of about 50 joules was developed to rapidly charge a 2.5μF capacitor bank which when discharged, ignited an EG&G FX98C-3 (3" length, 70mm diameter) flash lamp. The capacitor discharge was triggered by a standard square wave signal generator at the desired frequency. An oscilloscope sweep triggered by the release of the bubble breaking sphere from the electromagnet facilitated accurate monitoring of the flash, enabling the time at which each exposure was taken after bubble breaking to be accurately known. The flash was masked except

for two aligned slits to provide a pulsed vertical sheet of light directly above the bubble tube and normal to the line of sight of the camera. This illumination system permits particulate to be visible in only a cross-sectional slice (less than 1/2" wide) through each event allowing detailed visualization of the internal flow structure.

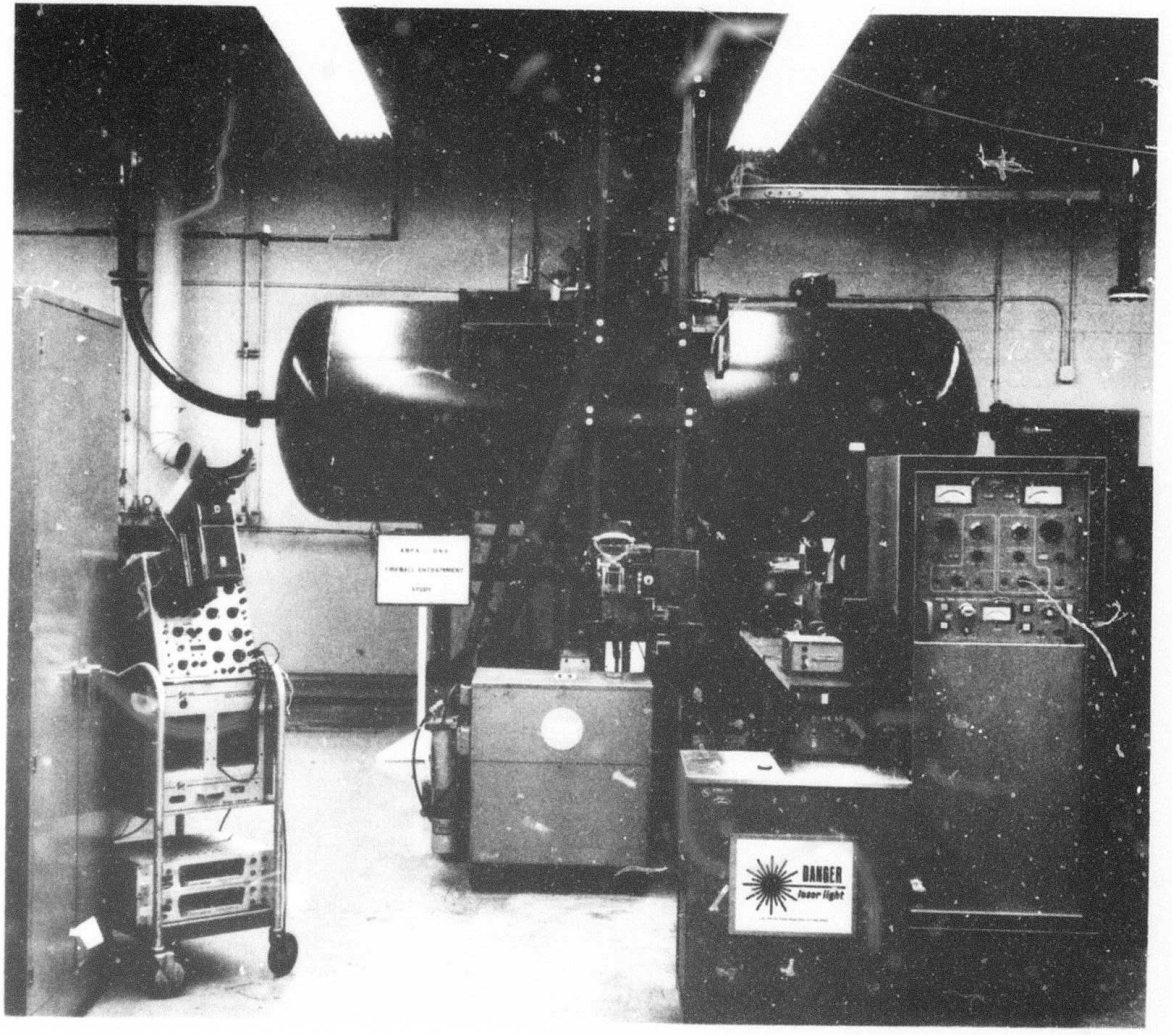

Figure 1. High Pressure Test Facility, Holocamera, and Support Equipment

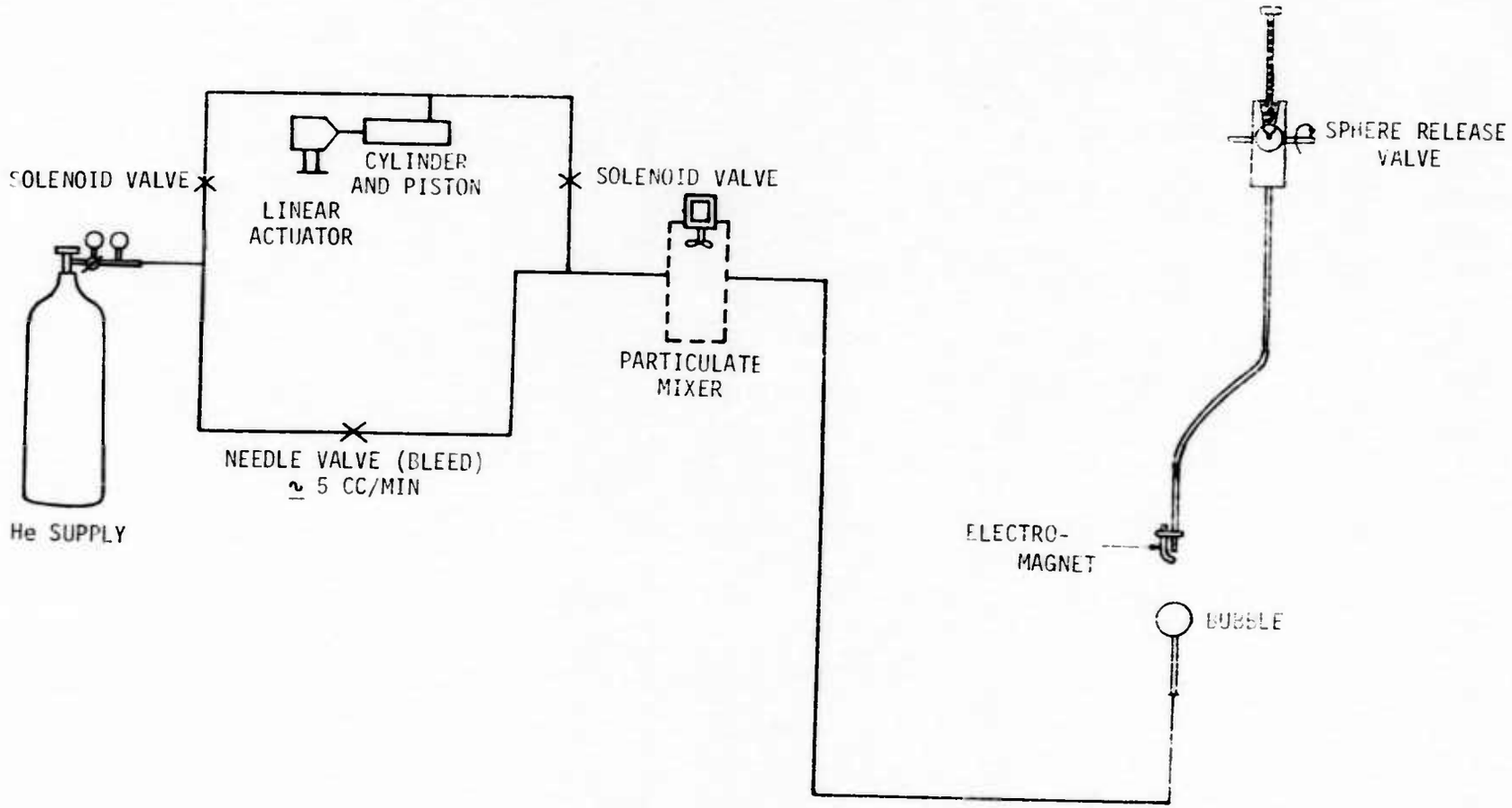

Figure 2. Schematic Diagram of Bubble Forming and Bursting Systems

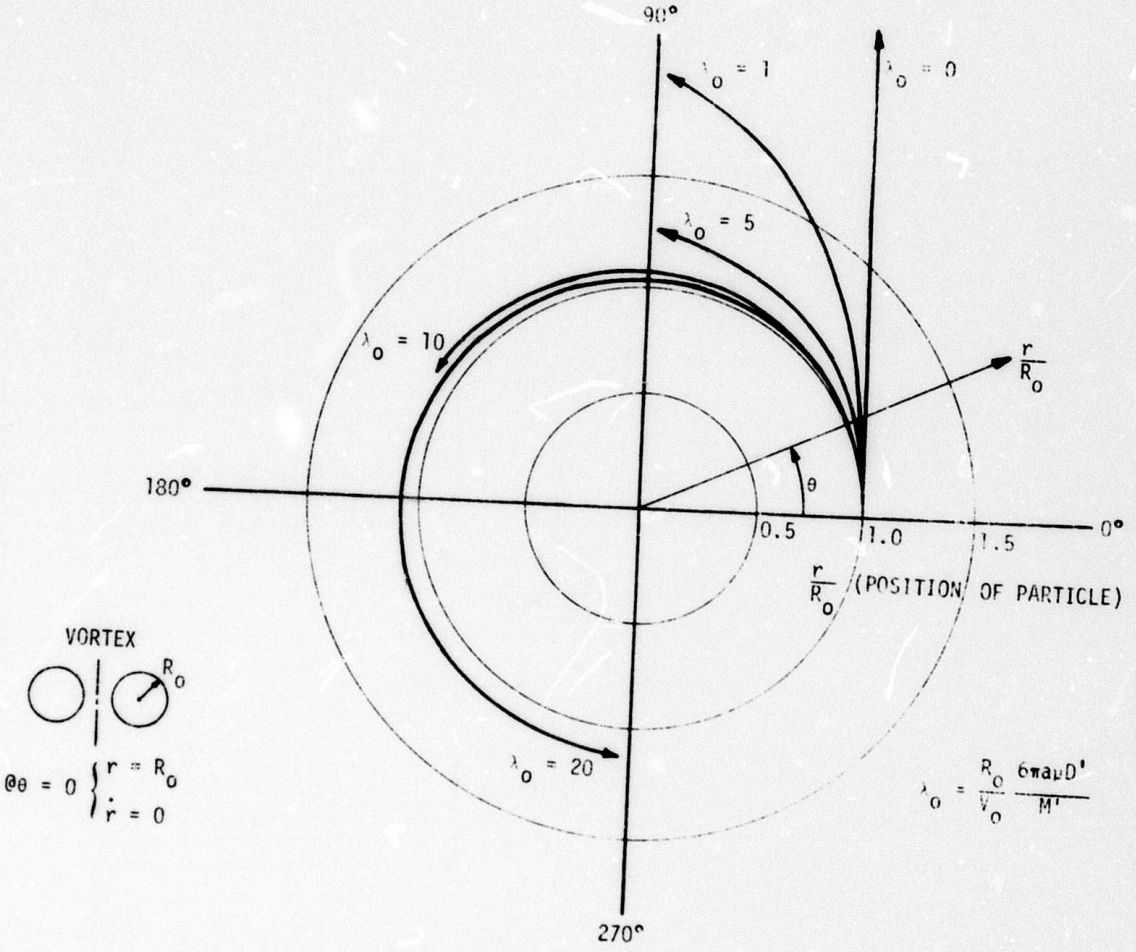

Figure 3. Dependence of Particulate Path on Parameter λ_o (Reference 2)

3. DATA ACQUISITION AND INTERPRETATION

In this section, acquisition and interpretation of finite fringe interferograms as well as particle tracking photographs will be discussed. The procedure used to obtain and interpret sets of infinite fringe interferograms of a simulated fireball was thoroughly discussed in Reference 1 and will not be repeated here.

3.1 ACQUISITION AND INTERPRETATION OF FINITE FRINGE INTERFEROGRAMS

A horizontal view finite fringe interferogram may be acquired using the same procedure as an infinite fringe interferogram as described in Reference 1 with one additional step. This step consists of a precise rotation of both the horizontal beam plate holder and its adjacent mirror between acquisition of the test and comparison records on the holographic plate.

An example of a finite fringe interferogram is presented in Figure 4. In this type of interferogram, the test disturbance causes a displacement or shift in the fringes relative to the undisturbed portion of the test section. The magnitude of the fringe shift is directly relatable to fringe number in infinite fringe interferograms and therefore to an integrated change in density or concentration along the optical path.

The bulk of the interferometry data to date have been obtained from infinite fringe interferograms at conditions such that a near optimum number of fringes were present from a data interpretation and reduction standpoint. Generally as the tank pressure was increased, the vortices were studied at a later time in their development, hence at a higher rise position. Present emphasis on interferometry data acquisition (see Section 6) focuses on conditions at which either too many or too few fringes would exist for interpretation and data analysis if the infinite fringe technique were used.

Even using the finite fringe arrangement, there still exist fringe spacing limitations. To yield nonambiguous data, the fringe shift in a given length of an event cannot exceed the number of fringes laid on the

undisturbed portion of the interferogram over that same length. A good example which illustrates a case where the fringe shift per unit length is greater than the fringe spacing per unit length is an interferogram of an unbroken bubble where very large fringe gradients are present near the edge of the bubble (Figure 5).

Experiments have recently been completed which define the operating range for the existing finite fringe interferometry apparatus. The maximum fringe spacing is about 2 fringes/inch which will be used for low pressure, high rise tests, while the minimum fringe spacing is about 20 fringes/inch, commensurate with high pressure, low rise events.

3.2 ACQUISITION AND INTERPRETATION OF PARTICLE TRACKING DATA

The procedure used to acquire photographs of particulate seeded vortices is very straightforward. After blowing the bubble and waiting a few seconds to allow any internal motion to damp out, the metal sphere is dropped from the electromagnet simultaneous with the initiation of the flash lighting system. An oscilloscope sweep is triggered by the electromagnet release and records the flashes as a series of spikes using the output of a photodiode mounted inside the tank. After the vortex is out of view, the flash is shut off and the film advanced for the next event.

Interpretation of particle tracking data in this sense is limited to detailed internal structure, and trajectory and growth observations of the rising fireballs. These particulate, shown in Section 2.2.1 to accurately follow the motion of the fluid, adequately illustrate whether or not a vortex possesses a laminar, wrap-up "jelly-roll" structure, or a turbulent, more thoroughly mixed structure. Unfortunately, since the vortex appears many times in a single multiple exposure photograph, the constraint of not having vortices overlap together with the difficulty of identifying individual particles precludes a direct measurement of the velocity field. Acquisition of velocity data (both mean and turbulent) at a space fixed point with a laser Doppler velocimeter (LDV) is discussed in Section 6.

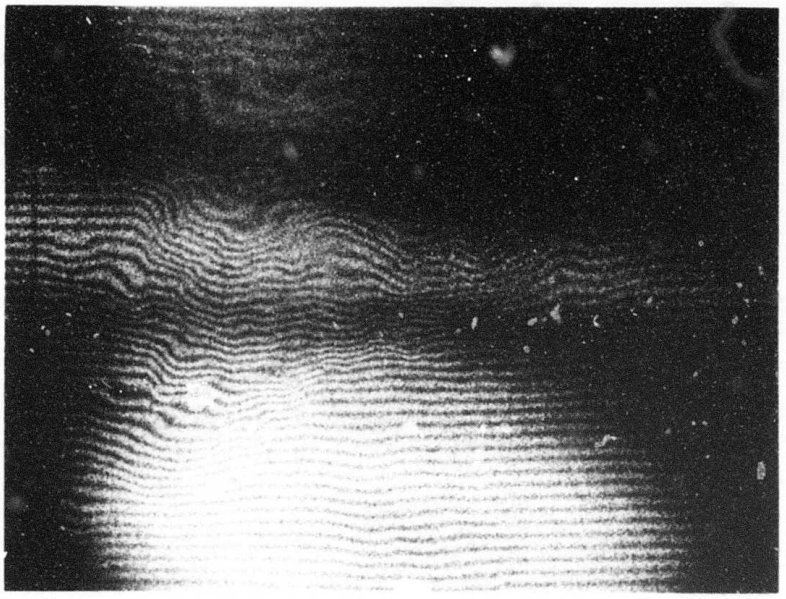

Figure 4. Typical Eight Atmosphere Finite Fringe Interferogram

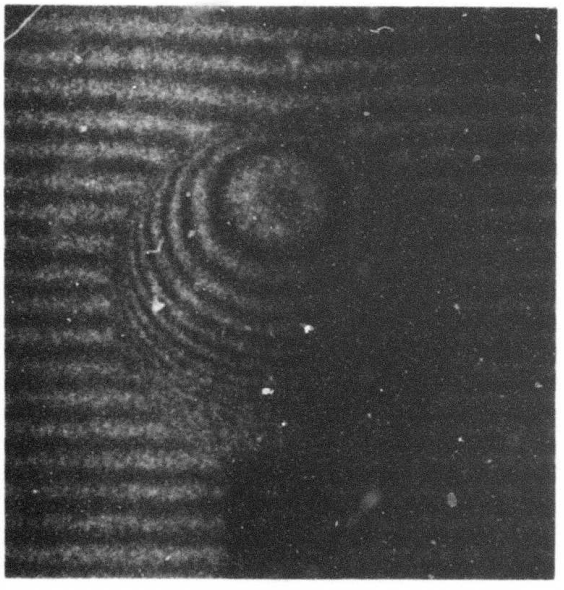

Figure 5. Finite Fringe Interferogram of Unbroken Bubble

4. DATA REDUCTION

The purpose of this section is to describe in detail techniques for reducing holographic interferometry and shadowgraph data as they apply to the present study.

4.1 HOLOGRAPHIC INFINITE FRINGE INTERFEROMETRY DATA

A data reduction technique has been developed (Reference 1), which will allow mean density and concentration (i.e., mass fraction) profiles to be calculated for a bimolecular mixing flow given a fringe distribution as a function of radius for an axisymmetric event. An examination of typical infinite fringe interferometry data (Figures 9, 10, 14, and 15) reveals that individual events are in general, asymmetric. It becomes obvious that an Abel inversion of the fringe shift equation

$$S = \frac{1}{\lambda} \int_0^L (n - n_\infty) ds$$

where S = fringe number or shift

λ = wavelength of light in vacuum

L = integration path length

n = index of refraction

ds = differential path length along the light ray

subscript

∞ = undisturbed conditions recorded in comparison scene and also observed in the test scene as a reference condition

is not valid when applied to individual interferograms such as these. To obtain an axisymmetric event, some type of average of these fringe distributions must be obtained. One could take an average in such a way to yield a probability-type result for density at a specified location in space, i.e., a tank-fixed approach. This would result in a very smeared

out* vortex which in no way would resemble a typical vortex. Instead, an approach was developed whereby a coordinate system would be established for each individual vortex based on the location of three points common to all vortices, but located in general differently from event to event. This approach retains the important physical features of the flow and produces a symmetric vortex which is a representative average vortex rather than a smeared out vortex average.

4.1.1 Establishment of Coordinates on Individual Interferograms

An interferogram is visually examined to determine the position of the saddle point by counting fringes inward from the edge of the vortex. In this connotation, the saddle point is defined as the point where the fringe number (see Section 4.1.2) simultaneously attains a maximum value in an axial direction and a minimum value in the radial direction. Two fringe maxima positions (generally having different fringe numbers) are determined in the same manner and an x-axis is drawn through them. The y-axis is then drawn orthogonal to the x-axis and through the saddle point. The point where the x and y-axes intersect becomes the vortex coordinate origin, or for the sake of brevity, simply the origin. Reference to Figure 6 will show that:

x_{LE} = distance from origin to first dark fringe on left side

x_{LM} = distance from origin to fringe maximum on left side

x_{RM} = distance from origin to fringe maximum on right side

x_{RE} = distance from origin to first dark fringe on right side

y_{sp} = distance from origin to saddle point

Tank-fixed parameters of purely statistical interest are:

η = rotation of x-axis from true horizontal

z_0 = vertical rise distance of origin from top of bubble tube

x_0 = horizontal distance from origin to center of bubble tube

*In the sense that the averaged event would be much larger than any individual vortex and the important edge gradients would be reduced.

4.1.2 Obtaining Fringe Profiles from Individual Interferograms

The center of each fringe is located and numbered where it intersects the x-axis defined in the previous section. The numbering starts with S = 1/2 for the outermost dark fringe (corresponding to the half-wavelength shift in optical path discussed in Section 4.2 of Reference 1), 1 for the next inward light fringe, and so on, increasing by 1/2 each time a new fringe is encountered. Care must be taken to give the same fringe the same number when it intersects the x-axis more than once. What results is m ordered pairs (x_{ij}, S_{ij}) $j = 1, 2, \ldots m$ for every i^{th} interferogram, $i = 1, 2, \ldots n$. The next section describes how an average fringe distribution is obtained over n interferograms.

4.1.3 Data Averaging

In the process of establishing an average vortex, it is essential to preserve the important physical features by normalizing the characteristic dimensions of each individual vortex. The dimensions selected for this purpose are the locations of the fringe maxima and the left and right edges relative to the origin.

To transform each event into a system of coordinates whereby maxima collapse onto the mean maxima and edges collapse onto the mean edges, the general linear transformation $\bar{x}_{ij} = ax_{ij} + b$ is used. First, the average locations of the edges and the maxima are computed using

$$\bar{x}_{LE} = \frac{1}{n} \sum_{i=1}^{n} x_{LE_i}$$

$$\bar{x}_{LM} = \frac{1}{n} \sum_{i=1}^{n} x_{LM_i}$$

$$\bar{x}_{RM} = \frac{1}{n} \sum_{i=1}^{n} x_{RM_i}$$

$$\bar{x}_{RE} = \frac{1}{n} \sum_{i=1}^{n} x_{RE_i}$$

The event is then divided into four regions as shown on the next page and the normalization is accomplished separately within each region.

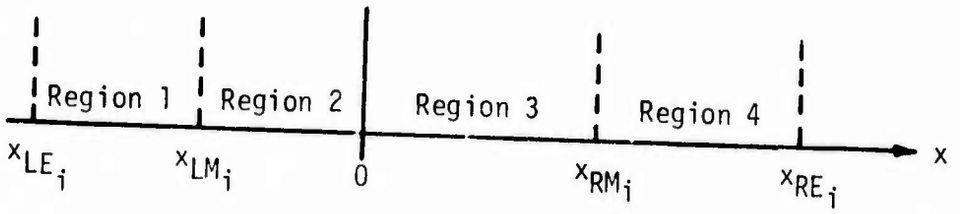

The constants for a and b in the general linear transformation are determined by matching the endpoints within each region to the averaged endpoints. For example, in region 1, at

$$x_{ij} = x_{LE_i},\ \bar{x}_{ij} = \bar{x}_{LE_i};\ \text{and, at } x_{ij} = x_{LM_i},\ \bar{x}_{ij} = \bar{x}_{LM_i}$$

For the j^{th} data point on the i^{th} interferogram, the new coordinates $\bar{x}_{ij}$ are:

In region 1,

$$x_{LE_i} \leq x_{ij} \leq x_{LM_i}$$

$$\bar{x}_{ij} = \frac{\bar{x}_{LE} - \bar{x}_{LM}}{x_{LE_i} - x_{LM_i}} x_{ij} + \bar{x}_{LM} - \frac{\bar{x}_{LE} - \bar{x}_{LM}}{x_{LE_i} - x_{LM_i}} x_{LM_i}$$

In region 2,

$$x_{LM_i} \leq x_{ij} \leq 0$$

$$\bar{x}_{ij} = \frac{\bar{x}_{LM}}{x_{LM_i}} x_{ij}$$

In region 3,

$$0 \leq x_{ij} \leq x_{RM_i}$$

$$\bar{x}_{ij} = \frac{\bar{x}_{RM}}{x_{RM_i}} x_{ij}$$

In region 4,

$$x_{RM_i} \leq x_{ij} \leq x_{RE_i}$$

$$\bar{x}_{ij} = \frac{\bar{x}_{RE} - \bar{x}_{RM}}{x_{RE_i} - x_{RM_i}} x_{ij} + \bar{x}_{RM} - \frac{\bar{x}_{RE} - \bar{x}_{RM}}{x_{RE_i} - x_{RM_i}} x_{RM_i}$$

Once all (x_{ij}, S_{ij}) have been transformed to $(\bar{x}_{ij}, S_{ij})$, there exist n S_{ij} vs. $\bar{x}_{ij}$ profiles with all edges occurring at $\bar{x}_{LE}$ and $\bar{x}_{RE}$, all maxima at $\bar{x}_{LM}$ and $\bar{x}_{RM}$, and the central minimum at $\bar{x} = 0$. These profiles may be averaged with respect to S at constant $\bar{x}$ to yield a mean $\bar{S}$ vs. $\bar{x}$ profile. It becomes readily apparent that every i^{th} distribution will not have discrete S at the same $\bar{x}$. What is done is to choose a convenient x_k to be used for each i^{th} event (say $\bar{x}_k = \frac{k}{L} \bar{x}_{LE}$, k = 1, 2, ... L) and linearly interpolate between $(\bar{x}_{ij}, S_{ij})$ and $(\bar{x}_{ij+1}, S_{ij+1})$.

$$S_{ik} = \frac{S_{ij+1} - S_{ij}}{\bar{x}_{ij+1} - \bar{x}_{ij}} (\bar{x}_k - \bar{x}_{ij}) + S_{ij}$$

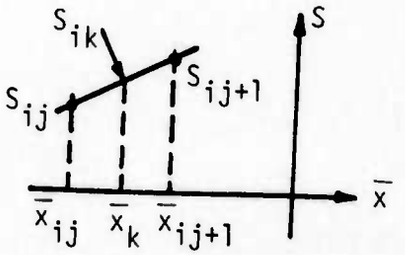

The input fringe numbers to the Abel inversion data reduction routine for an axisymmetric average vortex are simply $\bar{S}_k = \frac{1}{n} \sum_{i=1}^{n} S_{ik}$ for k = 1, 2, ...L. The $\bar{S}$ vs. $\bar{x}$ for both the left and right sides are computed, and provided that the number of events taken is sufficiently large, should for all practical purposes coincide. $\bar{S}$ is then extrapolated smoothly from 1/2 to zero to provide an outer radius of the vortex, required in the data reduction procedure.

The number of events n required to form an acceptable averaged event requires a compromise between the degree of asymmetry in the averaged event and effort required to acquire and reduce the data. One way to investigate how many events are required is to plot parameters indicative of asymmetry vs. number of events. The method used in this study is to calculate $\bar{x}_{LE}$, $\bar{x}_{RE}$, $\bar{x}_{LM}$, $\bar{x}_{RM}$, $\bar{S}_{LM}$, $\bar{S}_{RM}$ for different numbers of events used

and plot the differences in sides as a function of number of events; $\left(\frac{\overline{\Delta x_E}}{\bar{x}_E}\right), \left(\frac{\overline{\Delta x_M}}{\bar{x}_M}\right), \left(\frac{\overline{\Delta S_M}}{\bar{S}_M}\right)$ vs. n. When all of these parameters converge sufficiently close to zero, a satisfactory number of events have been included. Analysis of data obtained at both laminar and turbulent conditions indicates that a data set of 20 to 25 events is generally sufficient to satisfy this symmetry requirement.

4.1.4 Fireball Wake Interferometry Data Reduction

In addition to mean radial helium concentrations through the core of the vortex, radial helium concentrations at various positions through the fireball wake may be extracted from the interferometry data. One is confronted again as to what type of an averaging approach should be used and commensurate with the previous sections, a free coordinate system and normalization with respect to the wake edges were selected.

The coordinates are established in the following manner (refer to Figure 7): An axis approximating the center of the wake is determined by eye and drawn longitudinally through the core of the vortex. The wake coordinate origin becomes defined by a line drawn normal to the wake axis through the vortex coordinate origin (where it was defined in Section 4.1.1). All cuts through the wake are parallel to this line (normal to the wake axis) and their locations are based on fractions of vortex diameters below the wake origin.

Fringe numbers along these cuts are recorded in the same manner as was described in Section 4.1.2. The fringe profiles for the same z_w/D cuts are averaged over n interferograms using the edges and center as normalizing parameters, and when n is sufficiently large, a symmetric averaged fringe profiles results. Since the axial symmetry condition is once again satisfied, the previously discussed Abel inversion of the fringe shift equation may be applied to calculate radial helium concentrations.

4.2 HOLOGRAPHIC FINITE FRINGE INTERFEROMETRY DATA

The Abel inversion technique mentioned in Section 4.1 applies equally well to finite fringe interferograms, but the input $\overline{S}(\overline{x})$ are obtained in a different manner.

The procedure used to reduce finite fringe interferograms for a horizontal (in same direction as parallel fringes in undisturbed flow region) cut is as follows: First, by inspection, the fringe which has the maximum shift is determined. A tracing is then made following this fringe across the disturbed region. The fringe spacing can be measured so the vertical displacement of this fringe from the undisturbed may be expressed in number of fringes of shift. This continuous fringe shift as a function of x is identical to the discrete fringe number as a function of x for infinite fringe interferograms.

As long as each fringe may be continuously followed, it is very straightforward to extract several fringe distributions through each event. However, it should be noted that this simple data reduction is based on horizontal cuts through events which may not be aligned horizontally (see Section 4.1). Consequently, the flexibility inherent in the present infinite fringe data reduction procedure such as inclining the coordinate axes through the maxima is not possible with this simple finite fringe interpretation.

It is possible to reduce data along a line not parallel to the undisturbed horizontal fringes. Through a very thorough inspection, the two fringe maxima may be located (if the event is skewed these maxima will in general correspond to different fringes) and an x-axis can be drawn. Fringe shifts could then be measured on a fringe by fringe basis, and the data reduction would proceed as previously outlined for infinite fringe data in Section 4.1.1.

4.3 SHADOWGRAPH DATA

Shadowgraph movies are utilized in this investigation to study gross motions of the rising vortex such as size and rise. This information cannot be obtained with interferometry since that diagnostic is limited to obtaining data at one instant of time in each event. After acquisition and

processing, each shadowgraph film is projected on a large sheet of paper where the outline of the vortex may be traced frame by frame until the vortex disappears from the field of view. Since only gross features appear on a shadowgraph frame (change of illumination proportional to the second derivative of density rather than directly with density as is the case with interferometry), such distinct features as saddle point and maxima cannot be distinguished, but the outline of the edge can be accurately identified. While viewing the shadowgraph movies, one may quite accurately visually establish a radial axis through the center of each event. The data averaging procedure is outlined below.

Referring to Figure 8, one may define for the j^{th} frame of the i^{th} event

z_{ij} = rise height from top of bubble tube

D_{ij} = diameter of center of vortex

n_{ij} = inclination of diameter to horizontal

$x_{o_{ij}}$ = horizontal displacement of center of vortex from center of bubble tube

D_{o_i} initial bubble diameter

$j = 1$ is the first frame after the bubble is broken

The following physical parameters are averaged over n events to yield average quantities for every j^{th} frame:

$$\left(\overline{\frac{z}{D_o}}\right)_j = \frac{1}{n}\sum_{i=1}^{n}\frac{z_{ij}}{D_{o_i}}$$ mean normalized rise height

$$\left(\overline{\frac{D}{D_o}}\right)_j = \frac{1}{n}\sum_{i=1}^{n}\frac{D_{ij}}{D_{o_i}}$$ mean normalized diameter

$$\bar{n}_j = \frac{1}{n}\sum_{i=1}^{n} n_{ij}$$ mean rotation

$$\left(\overline{\frac{x_o}{D_o}}\right)_j = \frac{1}{n}\sum_{i=1}^{n}\frac{x_{o_{ij}}}{D_{o_i}}$$ mean normalized translation of center of vortex from bubble tube axis

Again, for a symmetric event, $\bar{\eta}_j$ and $\left(\frac{\overline{x_o}}{\overline{D_o}}\right)_j$ should approach zero as a cneck. In addition, standard deviations, σ are computed for each parameter where σ for some parameter P is defined as

$$\sigma_{P_j} = \left[\frac{1}{n}\sum_{i=1}^{n}(P_{ij} - \bar{P}_j)^2\right]^{1/2}$$

where

$$\bar{P}_j = \frac{1}{n}\sum_{i=1}^{n} P_{ij}$$

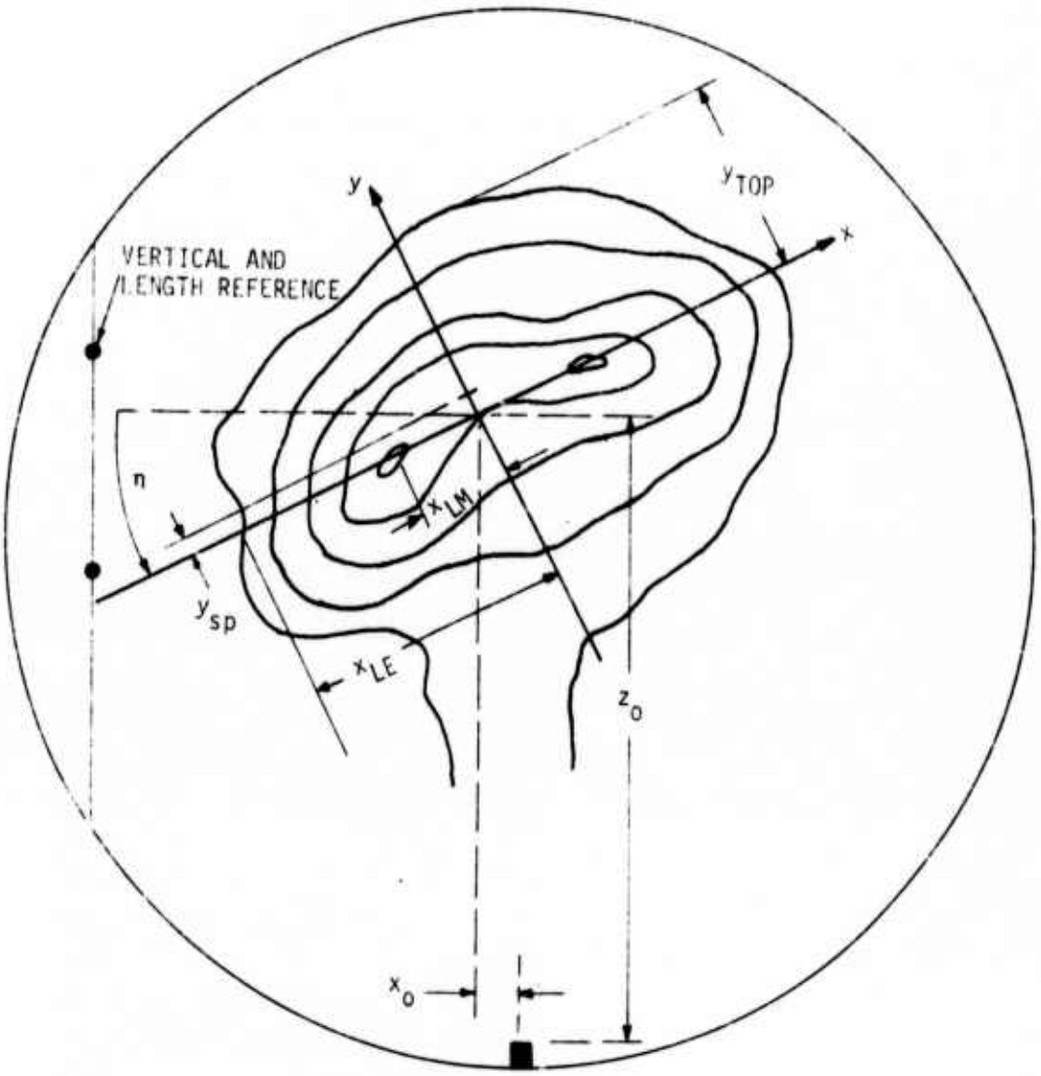

Figure 6. Nomenclature and Axes for Infinite Fringe Interferometry Data Reduction

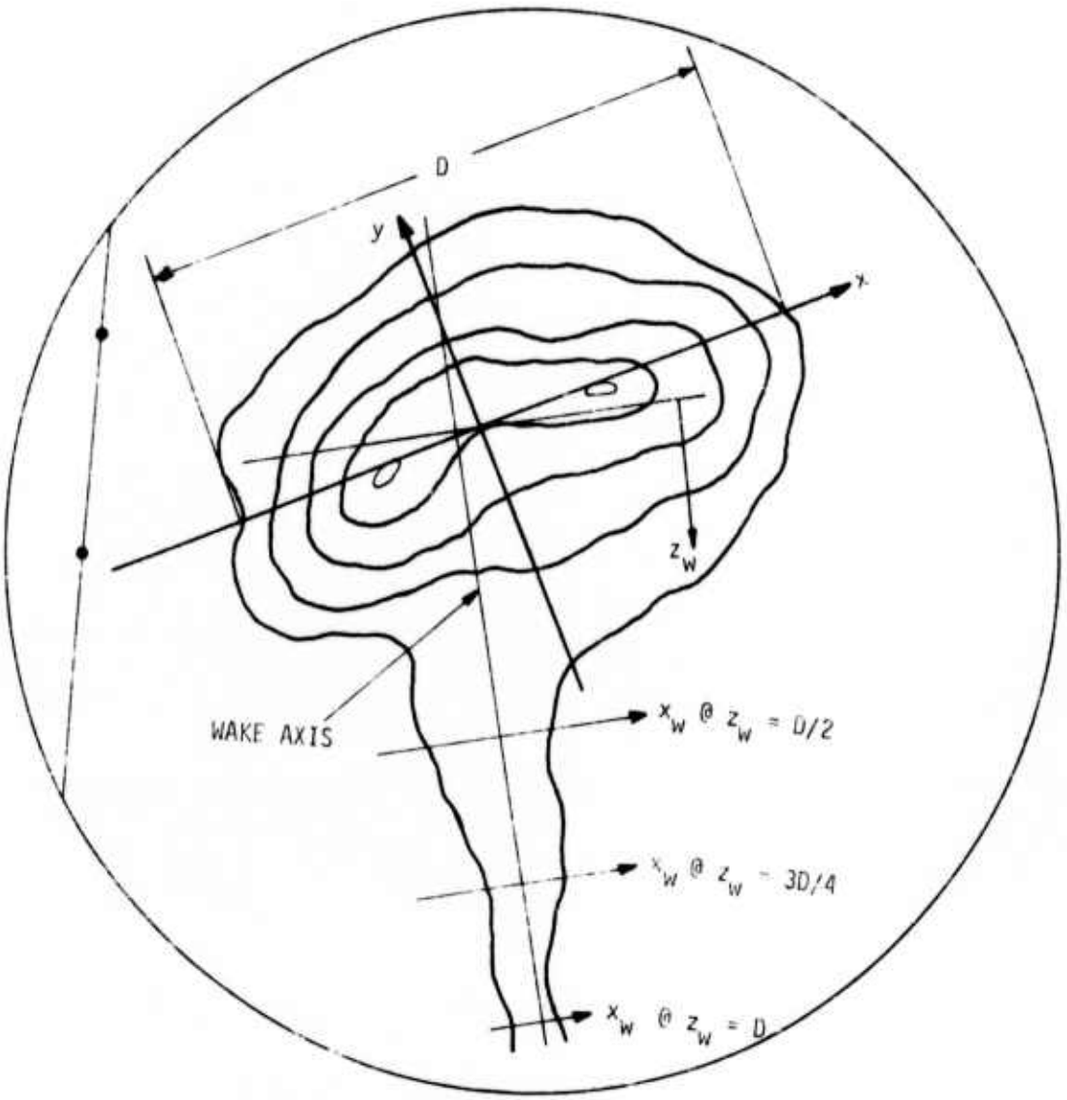

Figure 7. Nomenclature and Axes for Wake Data Reduction

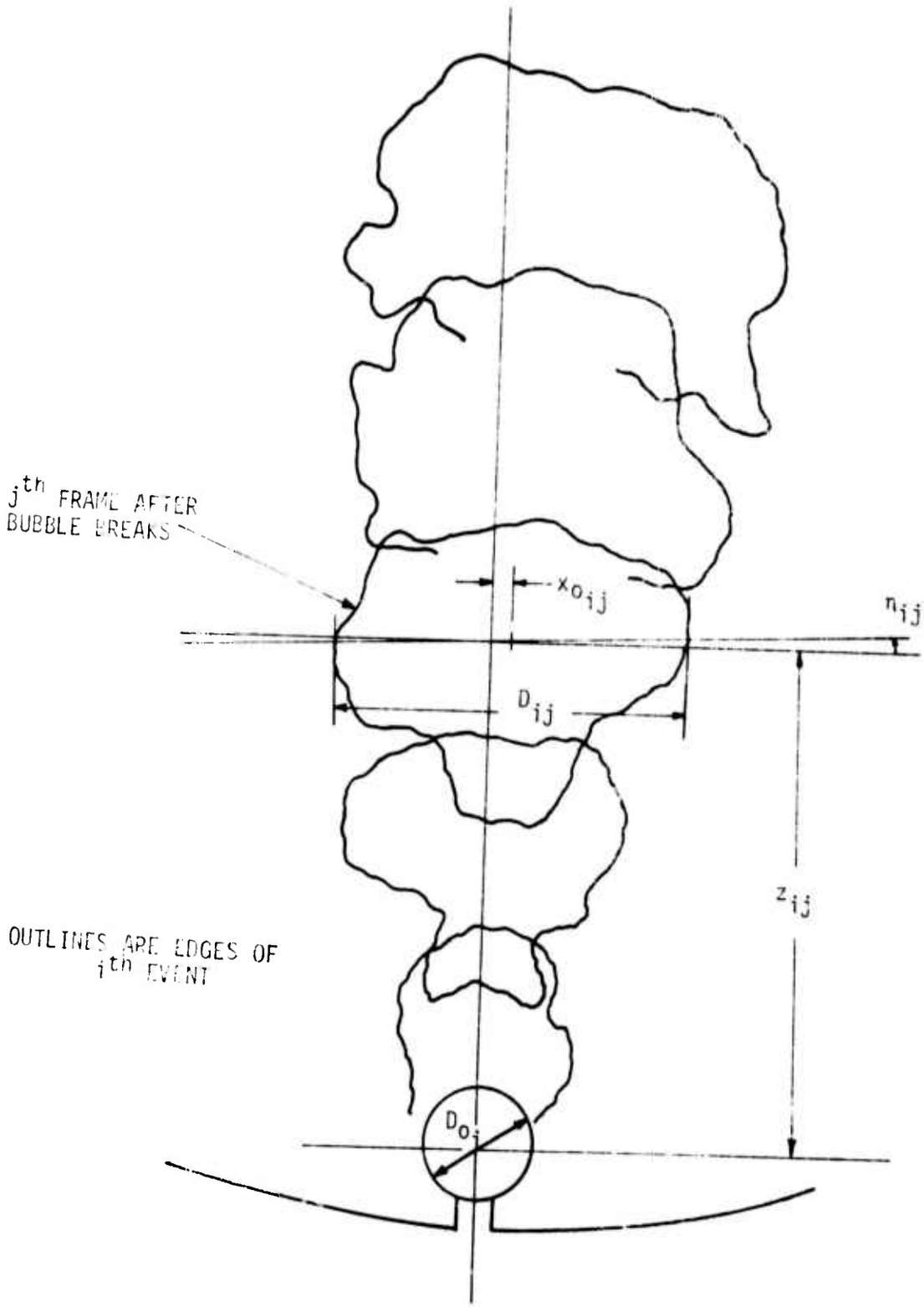

Figure 8. Nomenclature and Axes for Shadowgraph Data Reduction

5. EXPERIMENTAL RESULTS

A discussion of laminar and turbulent infinite fringe interferometry, shadowgraph, and particle tracking results are presented in the following sections.

5.1 HOLOGRAPHIC INTERFEROMETRY DATA

Unlike the interferometry results reported in Section 6.2 of Reference 1, it should be noted that all fringe distribution and helium concentration results presented in this section are based upon data acquired using the sphere drop bubble bursting technique described in Section 2.1 of this report and the new data analysis procedure outlined in Section 4.1.

5.1.1 Laminar Results

A total of 35 horizontal view holographic interferograms were obtained of separate repeat events at a tank pressure of one atmosphere, 0.19 seconds after bubble bursting. This tank pressure and the initial bubble diameter of 0.9 inch correspond to a Reynolds number of 1100. Two typical interferograms from this set are presented for comparison purposes in Figures 9 and 10.

Averaged radial fringe number profiles for left and right sides (using the method outlined in Section 4) are presented in Figure 11 and very nearly coincide, indicative of a very symmetric average event. This average event had a rise of 3.1 initial bubble diameters and a diameter of 2.22 initial bubble diameters.

Mean helium concentrations corresponding to these data are presented in Figure 12. Since helium concentration is dependent on the gradients of fringe number, wider discrepancies between left and right sides exist in the concentration profiles than in the fringe profiles, though they are still reasonably close. Note that the peak concentration of about 4 percent helium occurs at slightly less than half of the outer radius.

Radial helium concentrations along cuts through the vortex wake were calculated for the one atmosphere set of data at 1/2, 3/4 and 1 vortex diameter below the wake coordinate origin using the technique described in Section 4.1.4. The resulting mean concentration profiles computed from averaged fringe distributions are presented in Figure 13. Peak helium concentrations of approximately 2.5 percent exist near the center of the wake, become nearly a constant value of about 1.5 percent through most of the wake and reduce to zero rapidly at the edge. It is interesting to note that peak helium concentrations occurring at the wake axis are about half as large as the peak helium concentration within the vortex itself. Thus, even though only a small portion of helium forms the wake (the wake volume is far less than that of the vortex), it remains quite concentrated.

5.1.2 Turbulent Results

Thirty-three horizontal view holographic interferograms were acquired at a tank pressure of 8 atmospheres, 1.44 seconds after bubble bursting. The Reynolds number for these events was 10,400 based on this tank pressure and an initial bubble diameter of one inch. Two typical interferograms from this series are pictured in Figures 14 and 15.

Averaged fringe numbers vs. radius for these data appear in Figure 16. The degree of agreement between the left and right sides is less than that of the one atmosphere data, but nonetheless reasonably close. This average eight atmosphere vortex had a rise and diameter of 9.4 and 4.84 initial bubble diameters, respectively. The aforementioned limitations in the infinite fringe interferometry system prevented any complete analysis of a high pressure vortex at an earlier stage in development.

Mean helium concentrations as a function of normalized radius were calculated from these fringe distributions and are presented in Figure 17. The late stage in development of the vortex is reflected by the concentration profiles indicating little or no helium present within the central region approximately 0.4 times the outer radius of the vortex. The size, and the low peak helium concentration (compared to the one atmosphere case) are indicative of the late stage of development and resultant large volume of air entrained by the vortex.

5.2 SHADOWGRAPH SIZE/RISE STATISTICS

Twenty sets each of shadowgraph movies were obtained at a frame rate of 24 frames/second at pressures of 1, 4, 8, and 10 atmospheres to determine mean and standard deviation size/rise characteristics of simulated fireballs. They were averaged frame by frame using the procedure outlined in Section 4.3. Selected frames from a typical turbulent shadowgraph movie were previously presented in Reference 1.

Non-dimensional plots of rise vs. size are depicted on a logarithmic scale in Figure 18 for all four pressures. Additional interferometry data points and fireball size/rise data from an atmospheric nuclear test are also presented in this figure. Since fireball size and rise are among the better documented data from full scale nuclear events, an indication of the validity of this laboratory simulation may be inferred through a comparison with full scale data. It is apparent that the turbulent (eight and ten atmosphere) laboratory data are in excellent agreement with published results of at least one low yield, low altitude atmospheric nuclear test. Conversely, laminar and intermediate Reynolds number simulations reflect a much faster rise, resulting from a less pronounced entrainment of air than the turbulent events.

5.3 PARTICLE TRACKING RESULTS

Typical photographs of evolving particulate seeded vortices are presented in Figures 19 and 20 for comparison purposes and illustrate dramatically the effect of turbulence on toroid structure. Figure 19 represents a laminar vortex taken at a pressure of one atmosphere with an initial bubble diameter of one inch corresponding to a Reynolds number of approximately 1300. The important feature of this photograph is the distinct toroid "jelly-roll" structure apparent throughout the entire rise.

Figure 20 displays a turbulent event acquired at a pressure of eight atmospheres with the remaining test parameters identical to the one atmosphere photograph. The Reynolds number for this particular event was about 10,400. In this case, turbulent mixing has completely overwhelmed all internal structure evident in the laminar event. It is apparent from these and similar vortex structure photographs that a "jelly-roll" structure as such is strictly associated with a laminar event and will not exist in a full scale detonation.

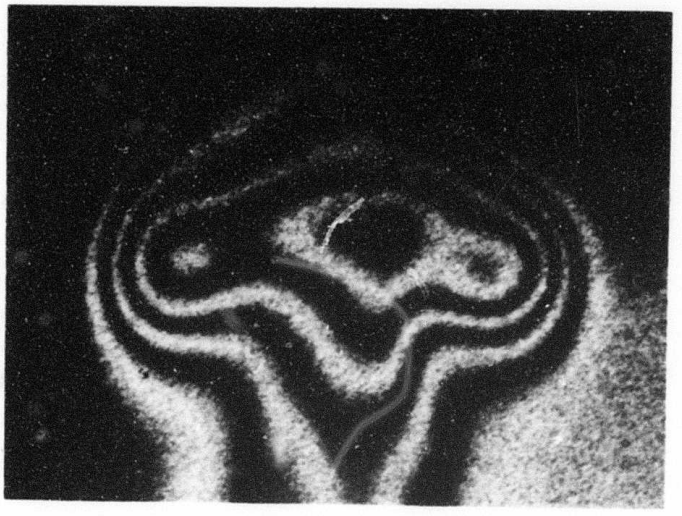

Figure 9. Typical Laminar Infinite Fringe Interferogram

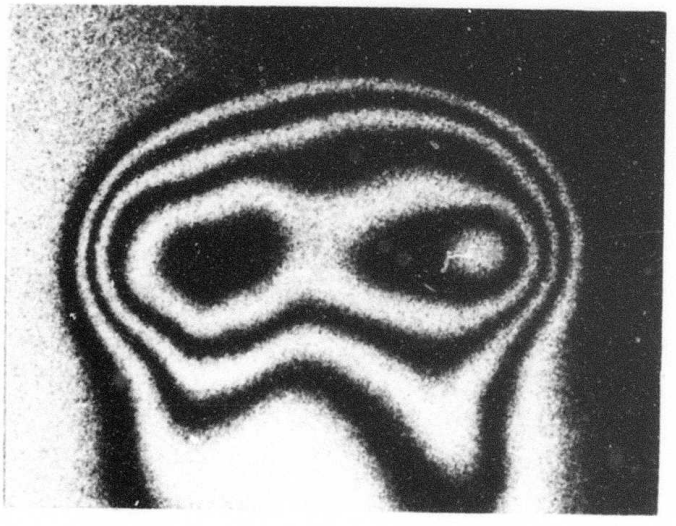

Figure 10. Typical Laminar Infinite Fringe Interferogram

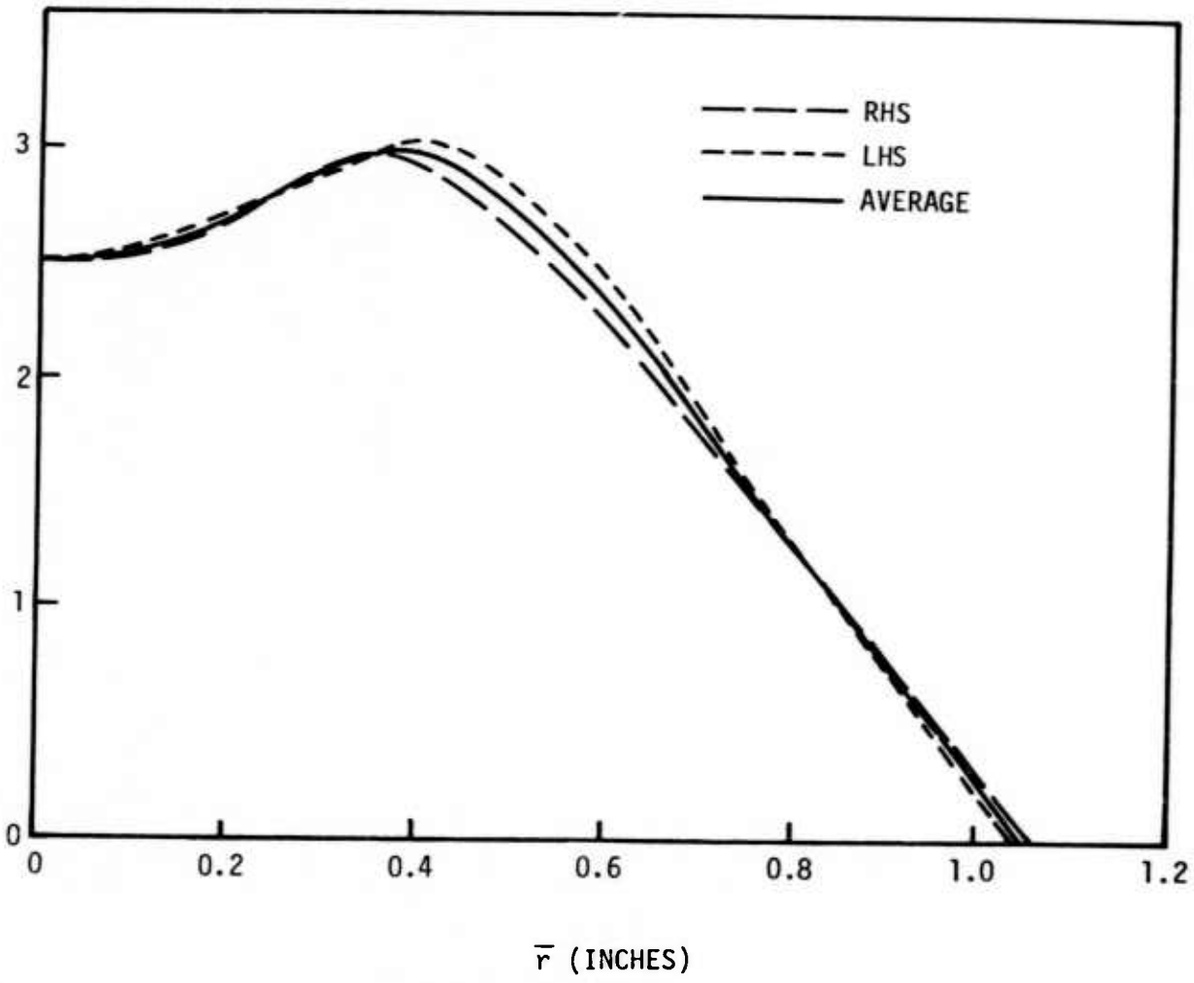

Figure 11. Averaged Radial Fringe Distributions - Laminar Data

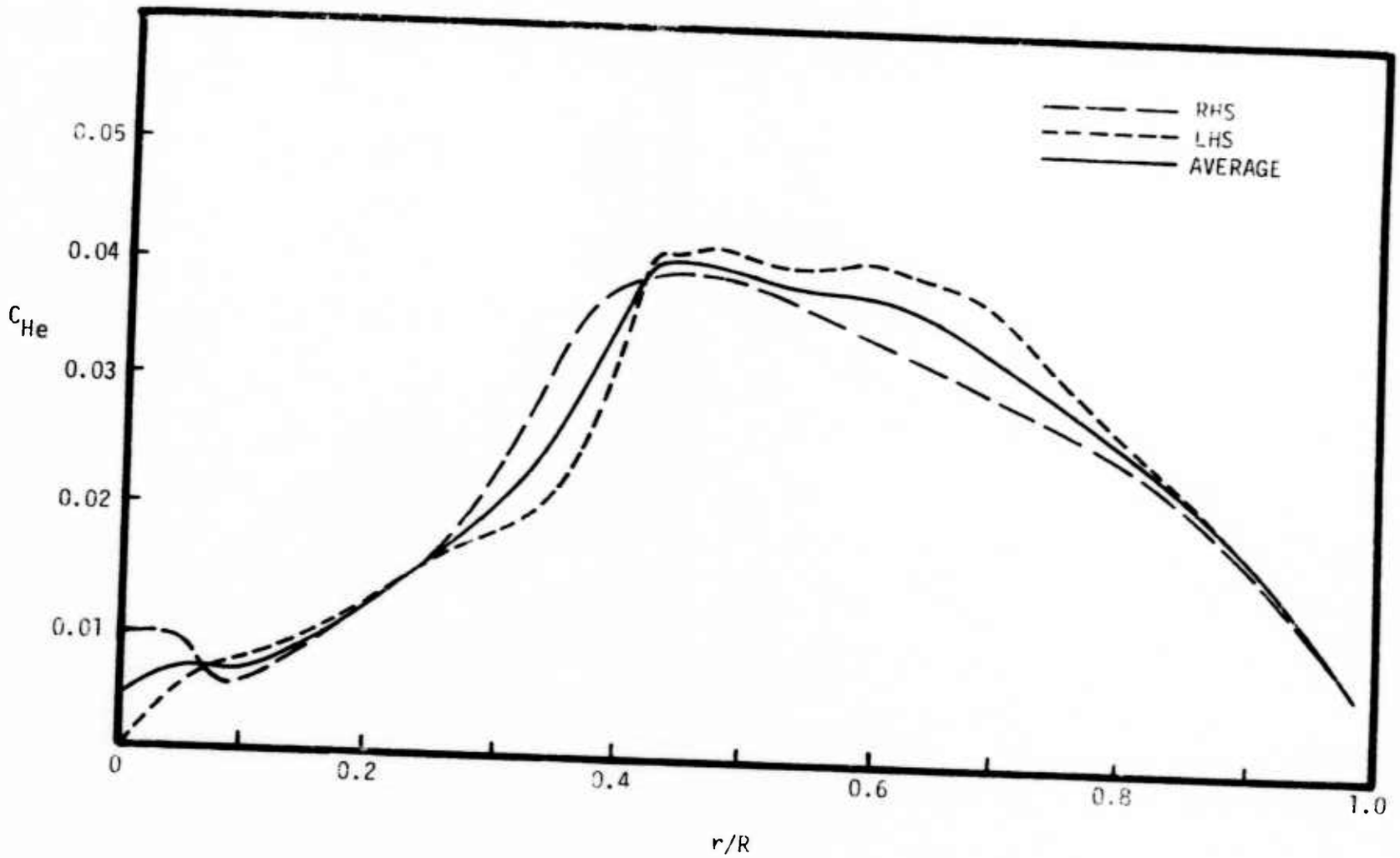

Figure 12. Averaged Radial Helium Concentrations - Laminar Data

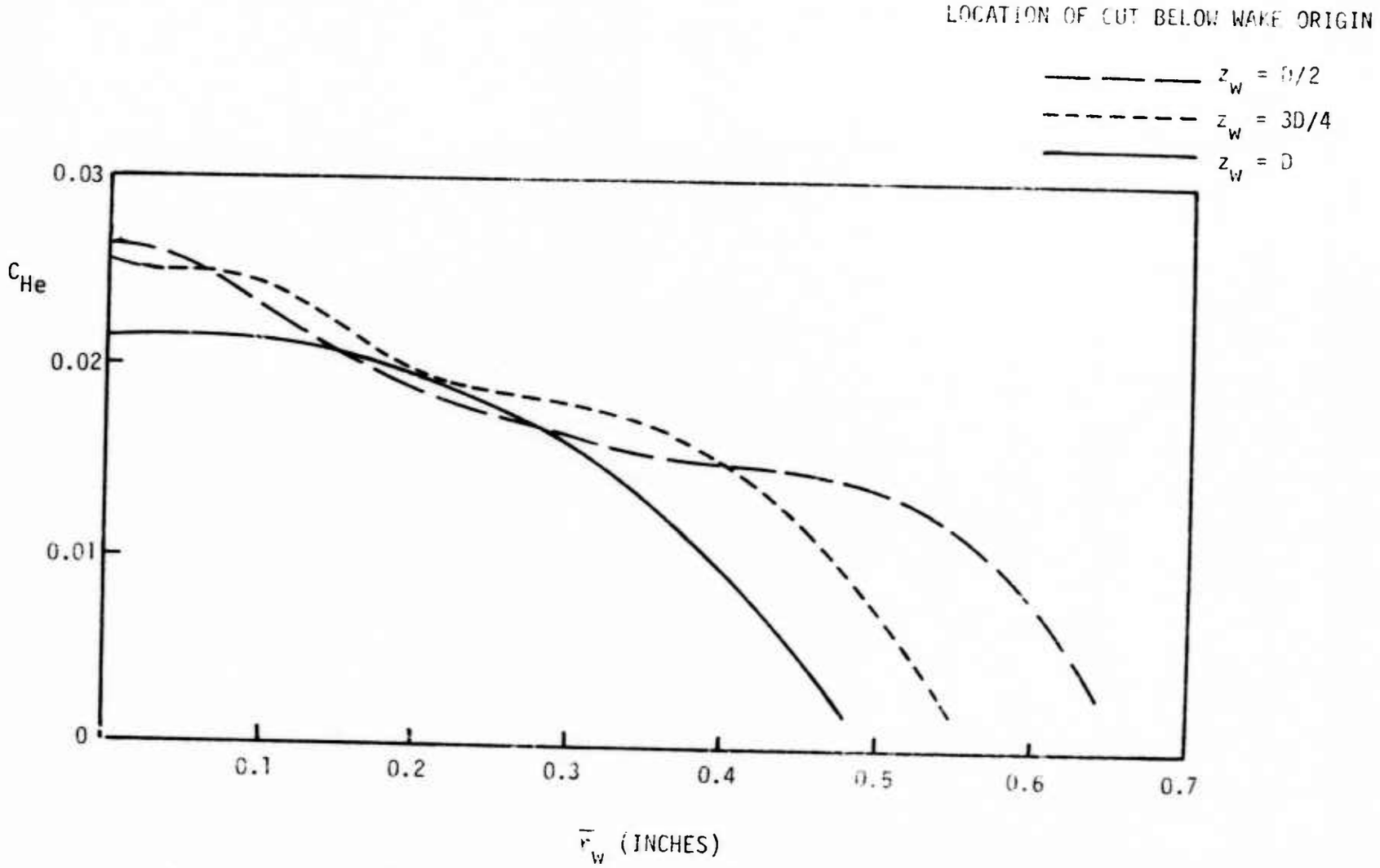

Figure 13. Averaged Laminar Fireball Wake Helium Concentration Profiles

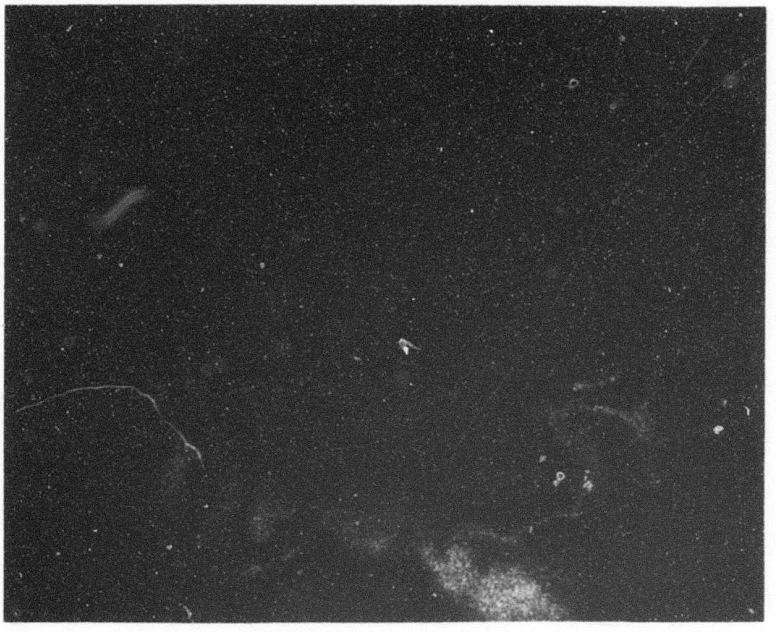

Figure 14. Typical Turbulent Infinite Fringe Interferogram

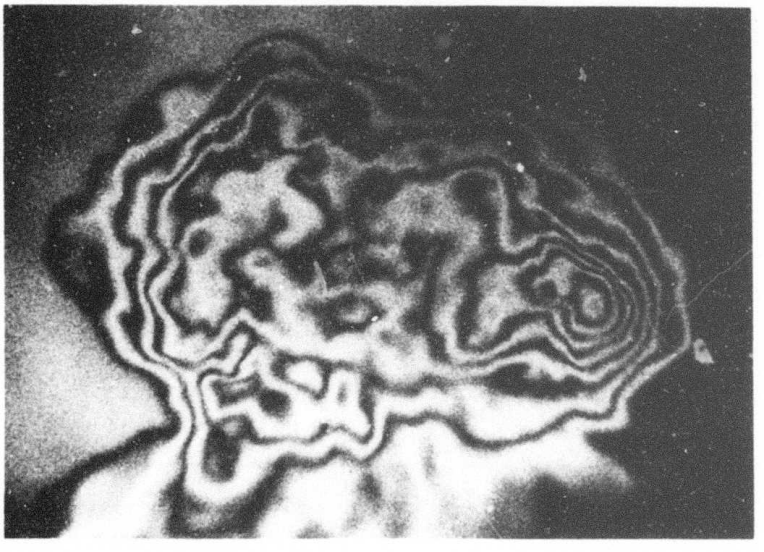

Figure 15. Typical Turbulent Infinite Fringe Interferogram

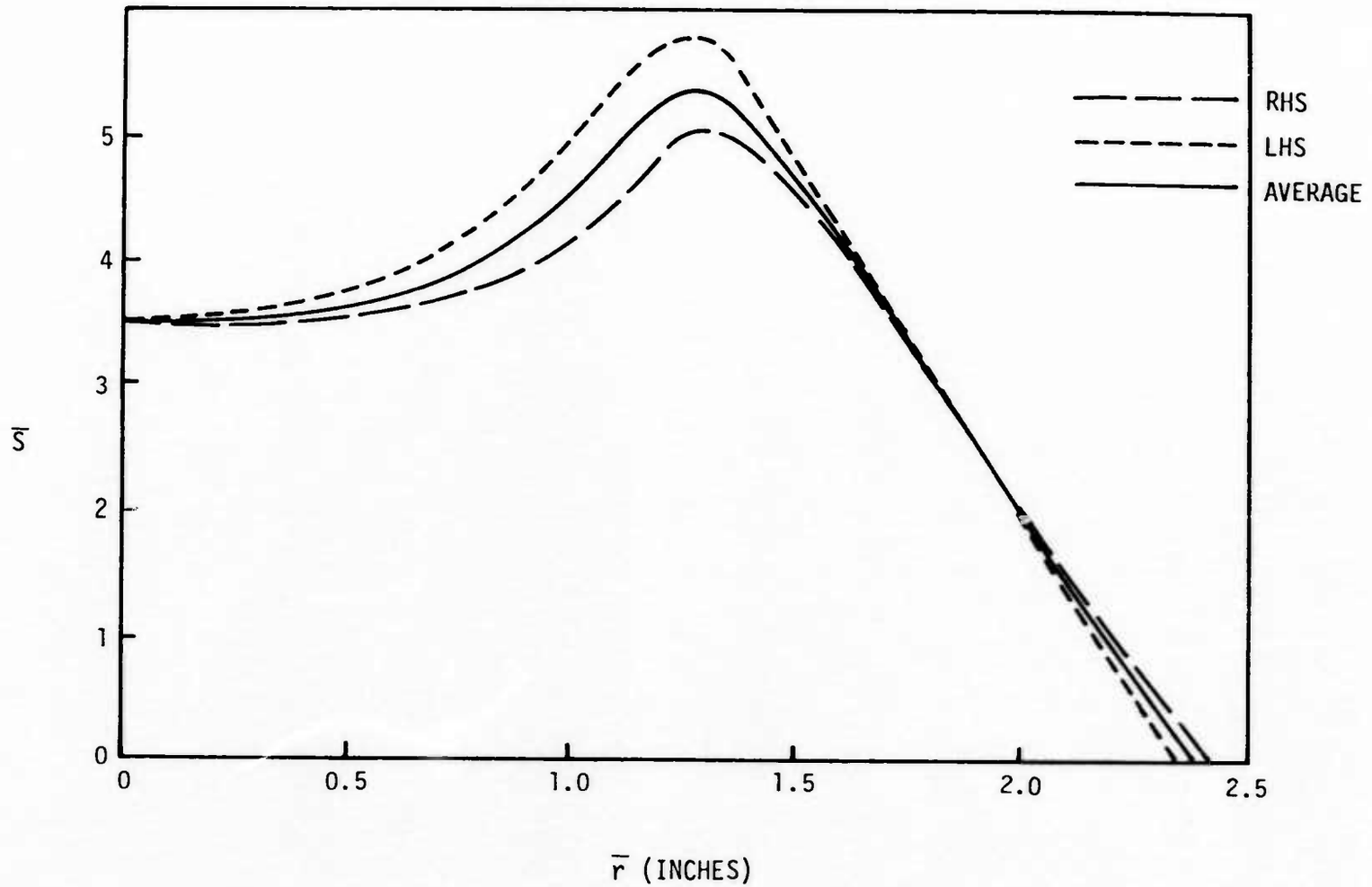

Figure 16. Averaged Radial Fringe Distributions - Turbulent Data

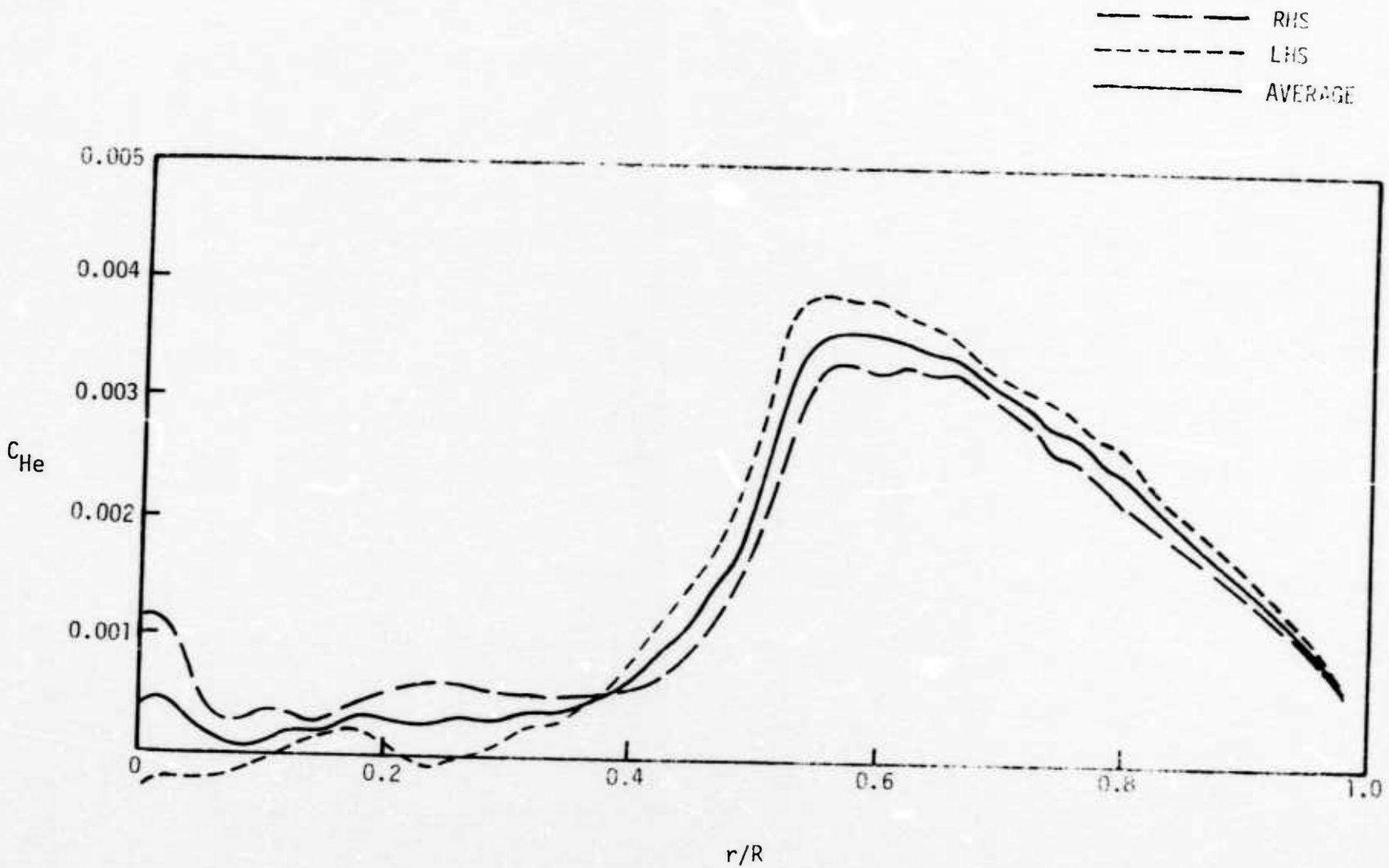

Figure 17. Averaged Radial Helium Concentrations - Turbulent Data

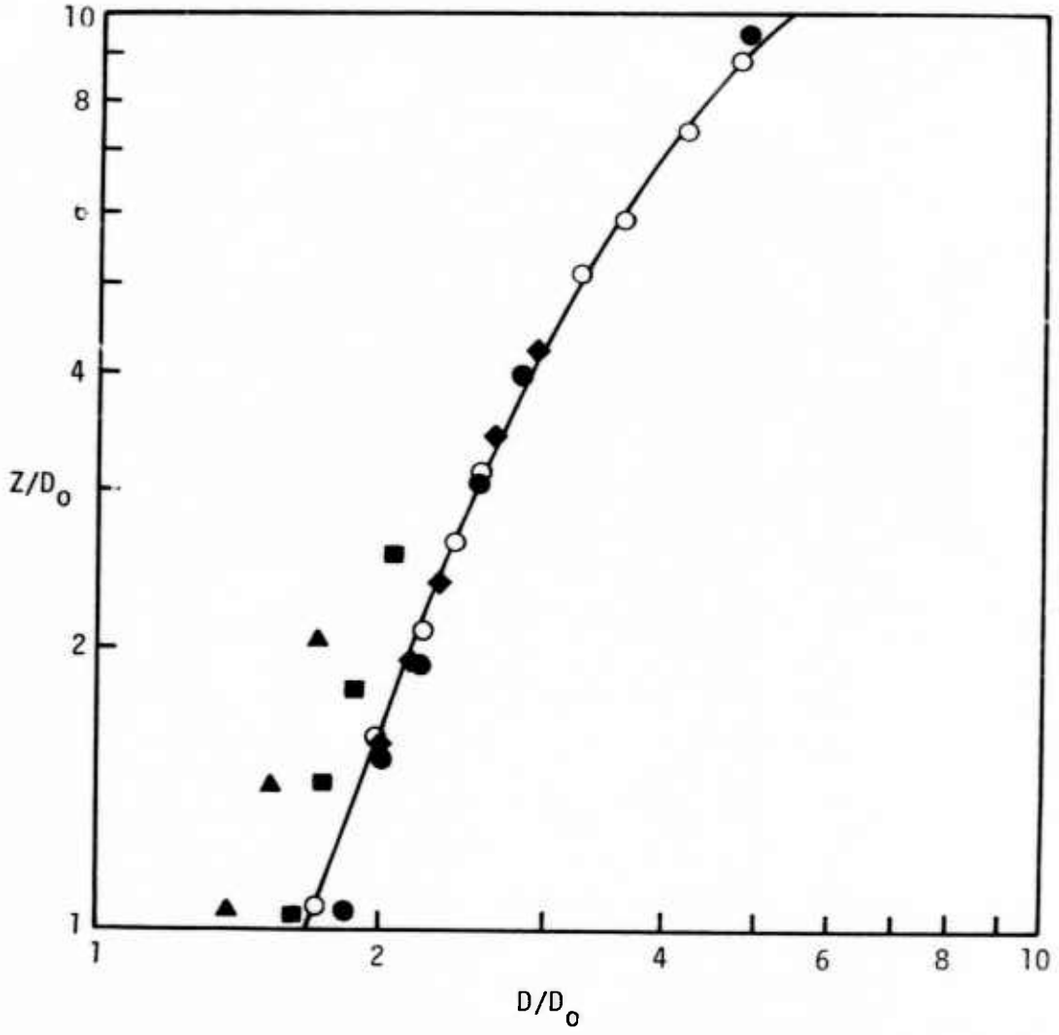

○ EVENT 1 LOW YIELD LOW ALTITUDE Re ∿ 5×10^8

◆ TRW 10 ATMOS. Re ∿ 13,000

● TRW 8 ATMOS. Re ∿ 10,400

■ TRW 4 ATMOS. Re ∿ 5,200

▲ TRW 1 ATMOS. Re ∿ 3,700

Figure 18. Fireball Size/Rise Characteristics

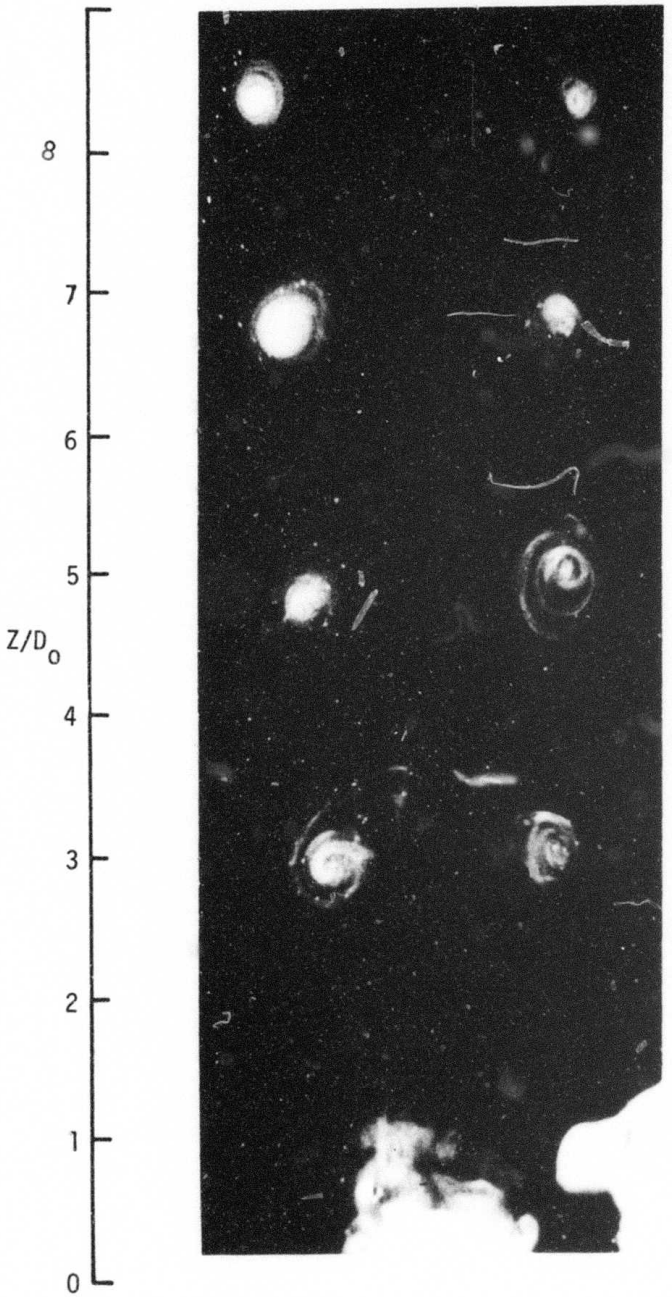

Figure 19. Multiple Exposure Photograph of Particulate Seeded Laminar Fireball

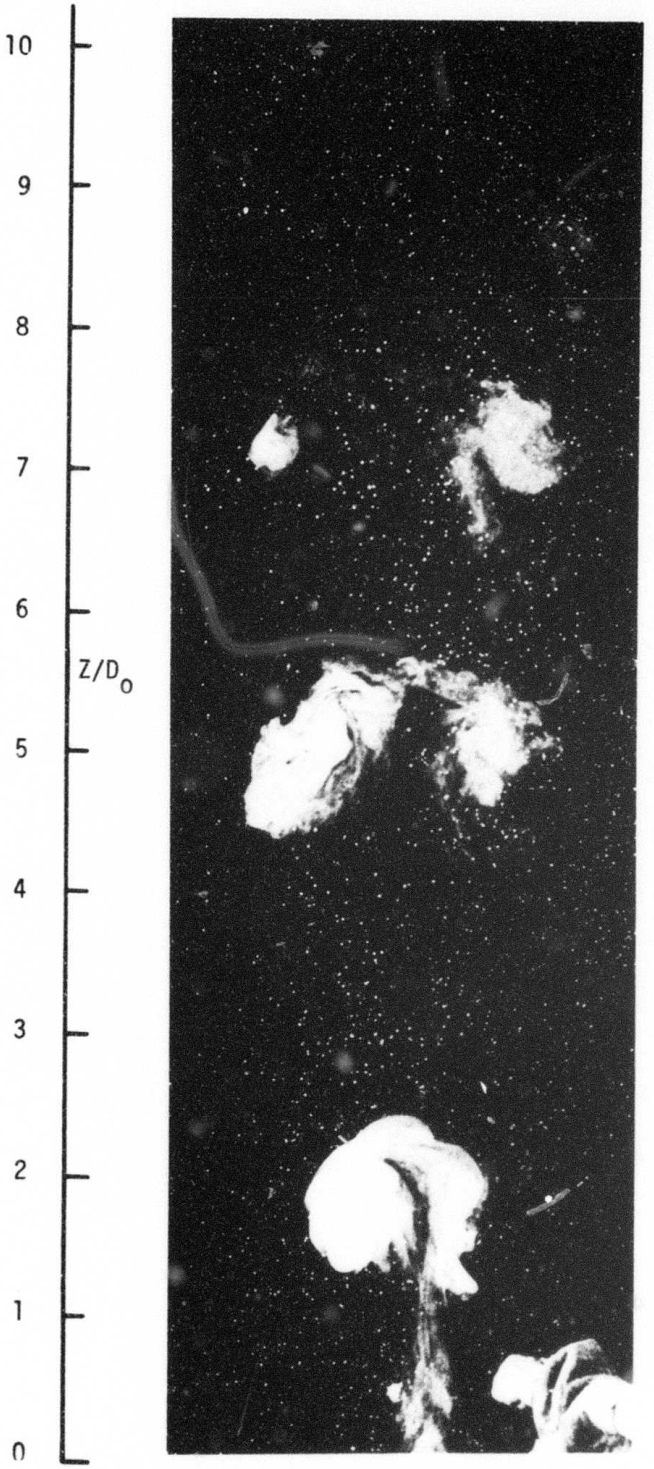

Figure 20. Multiple Exposure Photograph of Particulate Seeded Turbulent Fireball

6. CURRENT STATUS AND FUTURE PLANS

Within the fringe spacing capability of the finite fringe interferometer, 5 to 6 additional sets of interferometry data will be acquired and analyzed by the end of this phase of the study. They will consist of

(a) Minimum obtainable Reynolds number tests at low rise height and pressure to simulate the most laminar condition

(b) Maximum obtainable Reynolds number tests using N_2 bubbles in an SF_6 environment at ten atmospheres pressure

(c) Tests conducted at constant rise positions but different pressures to provide Reynolds number dependence information

These tests are currently in progress and results will be published in the final technical report during September 1973.

Direct turbulence measurements using the present diagnostic instrumentation are not possible, but an extension of the study is planned which will allow simultaneous velocity fluctuation and density fluctuation measurements to be made using a two-component laser Doppler velocimeter and a density probe, respectively. These essential measurements will be used to guide and provide inputs for the development of turbulence model equations for fireball flow fields.

7. REFERENCES

1. Haigh, W. W. and Mantrom, D. D., "Fireball Entrainment Study," Semi-Annual Report, TRW Report No. 18895-6002-RO-00, DNA 2981Z, August, 1972.

2. Wright, F. H., "The Particle-Track Method of Tracing Fluid Streamlines," JPL-PR-3-23, 2 March 1951.

3. Goldstein, S., ed., Modern Developments in Fluid Dynamics, Volume II New York: Dover Publications, Inc., page 492, 1965.